

pubs.acs.org/journal/abseba Article

Printable Nonenzymatic Glucose Biosensors Using Carbon Nanotube-PtNP Nanocomposites Modified with AuRu for Improved Selectivity

Tran N. H. Nguyen, Xin Jin, James K. Nolan, Jian Xu, Khanh Vy H. Le, Stephanie Lam, Yi Wang, Muhammad A. Alam, and Hyowon Lee*



Cite This: ACS Biomater. Sci. Eng. 2020, 6, 5315-5325



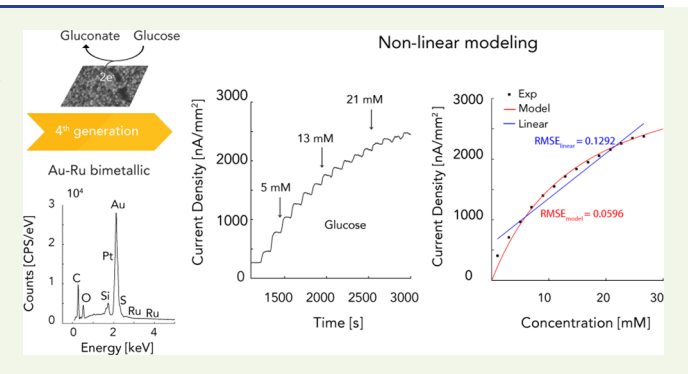
ACCESS

III Metrics & More

Article Recommendations

Supporting Information

ABSTRACT: Nonenzymatic glucose biosensors have the potential for a more reliable in vivo functionality due to the reduced risk of biorecognition element degradation. However, these novel sensing mechanisms often are nanoparticle-based and have nonlinear responses, which makes it difficult to gauge their potential utility against more conventional enzymatic biosensors. Moreover, these nonenzymatic biosensors often suffer from poor selectivity that needs to be better addressed before being used in vivo. To address these problems, here we present an amperometric nonenzymatic glucose biosensor fabricated using one-step electrodeposition of Au and Ru nanoparticles on the surface of a carbonnanotube-based platinum—nanoparticle hybrid in conductive



polymer. Using benchtop evaluations, we demonstrate that the bimetallic catalyst of Au-Ru nanoparticles can enable the nonenzymatic detection of glucose with a superior performance and stability. Furthermore, our biosensor shows good selectivity against other interferents, with a nonlinear dynamic range of 1-19 mM glucose. The Au-Ru catalyst has a conventional linear range of 1-10 mM, with a sensitivity of 0.2347 nA/(μ M mm²) \pm 0.0198 (n=3) and a limit of detection of 0.068 mM (signal-to-noise, S/N=3). The biosensor also exhibits a good repeatability and stability at 37 °C over a 3 week incubation period. Finally, we use a modified Butler–Volmer nonlinear analytical model to evaluate the impact of geometrical and chemical design parameters on our nonenzymatic biosensor's performance, which may be used to help optimize the performance of this class of biosensors.

KEYWORDS: direct ink writing, nonenzymatic glucose biosensor, bimetallic system, nonlinear modeling

■ INTRODUCTION

Over the years, enzymatic electrochemical biosensors based on glucose oxidase (GOx) have been popularized for the management of diabetes mellitus, owing to their good selectivity and high sensitivity. However, most of these enzyme-based glucose biosensors are disposable with limited functional lifetime. 1-4 One of the most recognized problems for the limited sensor lifetime is related to the intrinsic instability of enzymes. Although GOx is quite stable compared to others, enzymatic glucose biosensors are continuously exposed to the risk of thermal and chemical deformation during fabrication, storage, and usage. GOx rapidly loses activity below pH 2 or above pH 8, and it completely loses its functionality above 40 °C.5,6 Consequently, biosensor fabrication, including enzyme immobilization and device sterilization, requires a careful planning to prevent chemical- and temperature-induced enzyme inactivation.6

To circumvent the issue of enzyme degradation, significant efforts have been focused on investigating the electrocatalysis of glucose without using an enzyme as the biorecognition

molecule.⁷ The majority of nonenzymatic electrochemical glucose sensors generate an electrical current by directly oxidizing glucose on the electrode surface.⁸ Nanoscopic electrodes, especially nanoporous electrocatalysts, are frequently employed due to their high active surface areas.⁹ These are ideal for a kinetically controlled, surface-bound reaction such as direct glucose oxidation.^{10–12} Noble metal nanoparticles are often used for their excellent conductivity, catalytic properties, and large surface area to promote a good matrix for the bioadsorption of a molecule onto the surface.^{13,14} However, a major drawback of using single-metal metallic catalysts is that they oxidize various other endogenous interference species, such as L-ascorbic acid (AA), uric acid (UA), and 4-acetamidophenol

Received: May 1, 2020 Accepted: July 22, 2020 Published: July 27, 2020





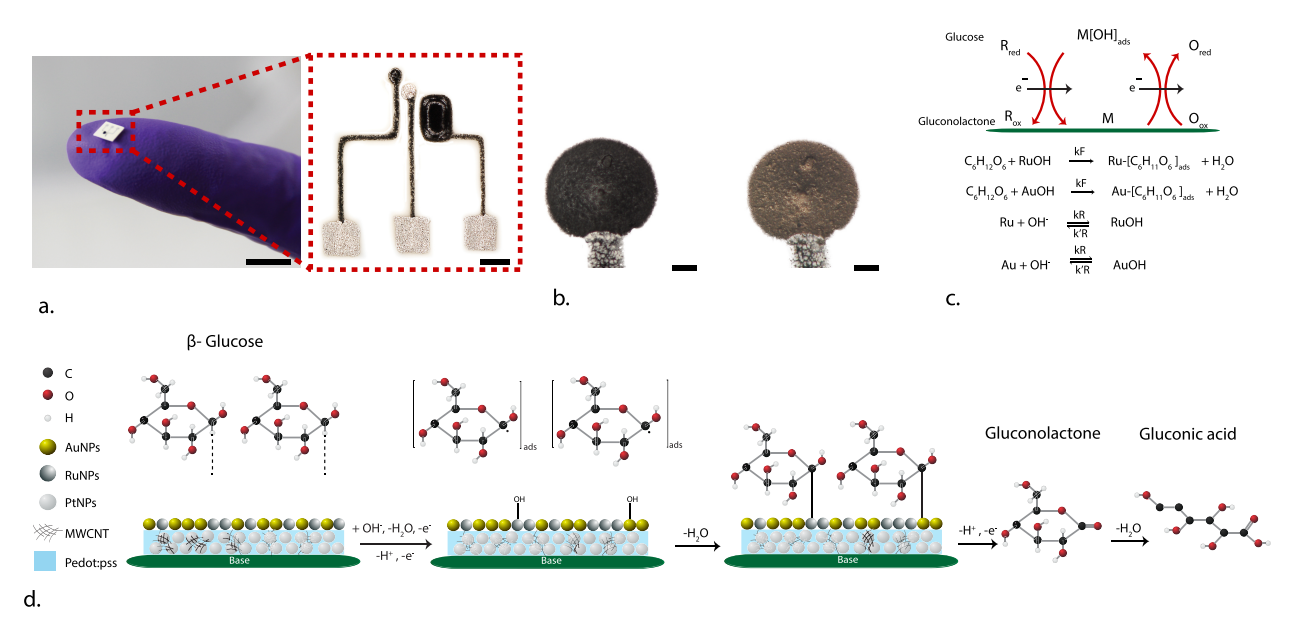


Figure 1. (a) Photographs of a flexible nonenzymatic glucose biosensor on a LCP sheet (scale bars, 10 mm and 500 μ m). (b) Photographs of the nanocomposite before (left side) and after the electrodeposition of Au-RuNPs on the surface (right side) (scale bars, 200 μ m). (c and d) Schematic illustration of the possible mechanism for the electrocatalytic oxidation of glucose at Au-RuNPs on the MWCNT-based nanocomposite surface, along with possible chemical reactions between the metal nanoparticle surface and glucose molecules.

(AP), in the potential range, similarly to direct glucose oxidation, resulting in poor selectivity.

Bimetallic alloys of nanoparticles are promising alternatives to achieve better selectivity because they oxidize glucose at a lower potential. ^{15–17} In addition, they are known for their superior electrocatalytic activity compared to single metal catalysts. ^{18–21} Thus, here we used electrodeposition of gold—ruthenium alloy nanoparticles (Au-RuNPs) to create a bimetallic coating to fabricate a more selective nonenzymatic glucose biosensor. Electrodeposition is a simple modification process that can produce a high-purity surface with a controllable particle size. ²² The combination of Au and Ru in Au-RuNPs synergistically enhances the oxidative current from glucose and improves the selectivity compared to a single-metal system. Their synergistic effect is due to their surface electronic states, which are greatly affected by changes in geometric parameters. ^{23,24}

Moreover, the supporting materials also play a major role in the performance of electrocatalysts due to their interactions, which facilitates the catalytic activities between metallic catalysts and support materials. To achieve a fine dispersion and high utilization, nanocatalysts are usually supported on high-surfacearea materials such as carbon nanotubes (CNT), carbon nanofibers, graphene, or activated carbon. This is due to the distinctive characteristics of such new carbon nanomaterials, such as more crystalline structures, high electrical conductivities, excellent corrosion resistances, and high purities. Hence, in this study, we employed our previously developed high-surfacearea Pt-nanoparticles (PtNPs) CNT-based nanocomposite electrodes, as an effective supporting material for one-step electrodeposition of AuNPs and RuNPs for direct oxidation of glucose. The supporting material for one-step electrodeposition of AuNPs and RuNPs for direct oxidation of glucose.

We used field-emission scanning electron microscopy (FESEM), X-ray photoelectron spectroscopy (XPS), energy dispersive X-ray spectroscopy (EDX), cyclic voltammetry (CV), and amperometry to verify the structural and electrochemical properties of Au-RuNPs catalysts. We also investigated the effects of different electrodeposition times and Au-RuNPs

catalyst compositions on the electrocatalytic activity and sensitivity to glucose. We found that our bimetallic system simultaneously has a good sensitivity and a wider dynamic range than previously developed nonenzymatic sensors. We employed a nonlinear model to correlate the geometrical and chemical design parameters to the amperometric response of the sensor. This model confirmed our choice of using a Au-RuNP catalyst rather than other types of electroactive surfaces, including Pt—Ru or PtNPs-based (single metal catalyst) biosensors. Finally, we showed that this new nonenzymatic glucose biosensor has good stability, reproducibility, and selectivity, which may be suitable for in vivo glucose detection in the future.

EXPERIMENTAL SECTION

Chemicals. Gold(III) chloride hydrate (HAuCl₄·xH₂O, ~50% Au basis), ruthenium(III) chloride hydrate (RuCl₃:xH₂O, 99.98% trace metals basis), chloroplatinic acid hydrate (H₂PtCl₆· xH₂O, > 99.9% trace metal basis), poly(3,4-ethylenedioxythiophene) polystyrene sulfonate (PEDOT:PSS) (5 wt %), and platinum nanoparticles (<50 nm particle size) were obtained from Sigma-Aldrich (St. Louis, MO). Carboxylic-functionalized multiwalled carbon nanotube (COOH-MWCNT; outer diameter, 10–20 nm; length, 10–30 μ m; purity, > 95 wt %) were bought from Cheap Tubes, Inc. (Grafton, Vermont). Sulfuric acid (H₂SO₄, 95–98%), 0.1 M phosphate buffer solution (PBS, pH 7.4), dimethyl sulfoxide (DMSO), D-glucose, sucrose, lactose, and fructose were obtained from Fisher Scientific (Waltham, MA). Ascorbic acid (AA), uric acid (UA), and 4-acetamidophenol (AP) were purchased from Alfa Aesar (Thermo Fisher Scientific, Waltham, MA). Ag and Ag/AgCl ink (CI-1001) were purchased from Engineered Conductive Materials, Inc. (Delaware, OH). Elastomeric polydimethylsiloxane (PDMS, Sylgard 184) was purchased from Dow Corning (Midland, MI). Ecoflex (00-30) was purchased from Smooth-On (Macungie, PA). Deionized water (DI) was purified using Milli-Q (Millipore, Bedford, MA). Basal glucose concentrations from the whole blood and human serum were measured with test strips and a glucometer (DS-W, Auvon, Peachtree Corners, GA). Whole porcine fresh blood ([glucose] = 2.585 mM) was collected from the animal facility of the Biomedical Engineering Department at Purdue University. It was mixed with 10 USP units of heparin/mL and stored at 4 °C until measurements were taken. Human serum ([glucose] =

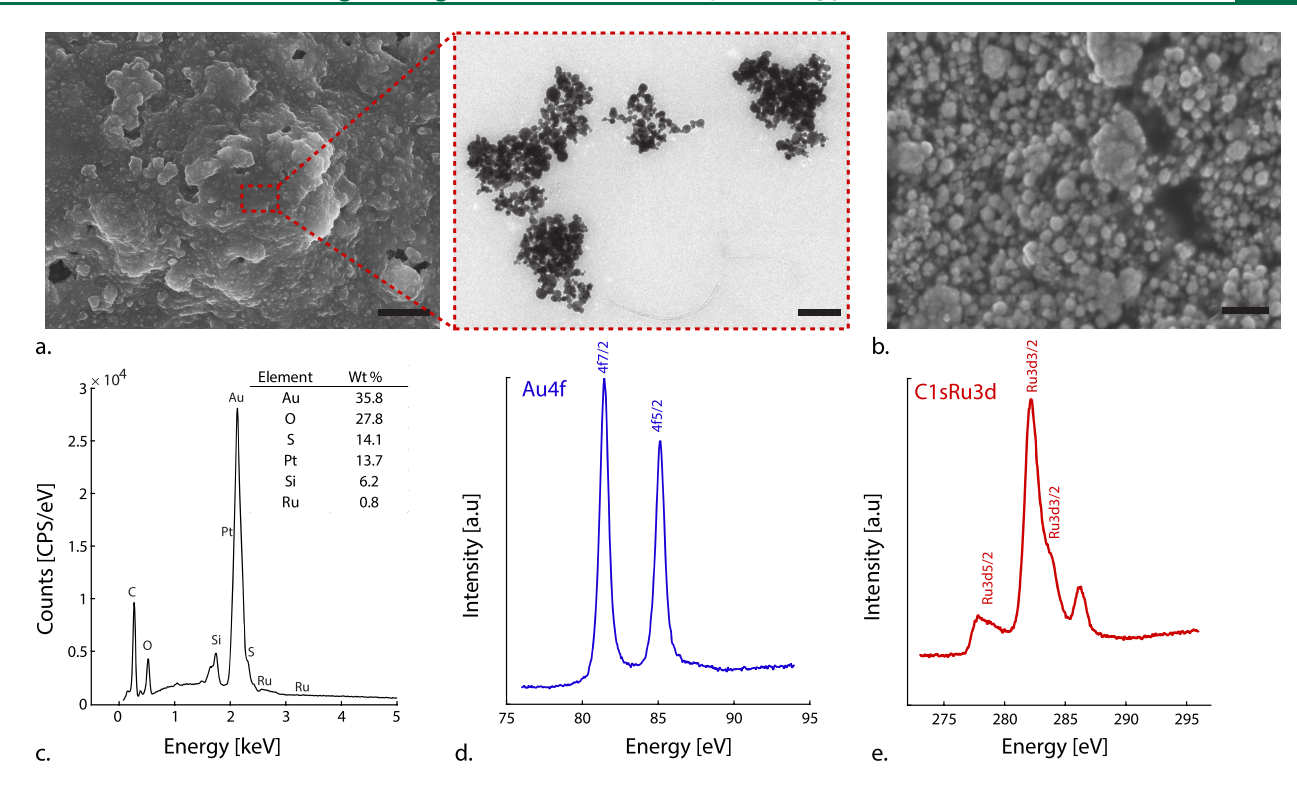


Figure 2. (a) Scanning electron micrographs of the nanocomposite (scale bars, 5 μ m). Inset shows the transition electron micrographs of a MWCNT-based nanocomposite (scale bar 200 nm). (b) Scanning electron micrographs of Au–Ru nanoparticles on a MWCNT-based nanocomposite (scale bar, 250 nm). (c) EDX spectrum of a fabricated Au-RuNPs-nanocomposite. XPS spectra of a Au-RuNPs-nanocomposite: (d) Au 4f and (e) C 1s-Ru 3d.

4.785 mM) from human male AB plasma was obtained from Sigma-Aldrich (H4522, St. Louis, MO).

Apparatus and Electrochemical Measurements. Electrochemical preparation of the sensors and in vitro experiments were conducted using a commercial benchtop potentiostat (SP-200, Biologic USA, LLC, Knoxville, TN, USA). All electrochemical evaluations were performed in 0.01 PBS (pH 7.4, 50 mL for all experiments). A conventional three-electrode cell was used for electrodeposition, with the prepared nanocomposite as the working electrode, the silver/silver chloride (Ag/AgCl/NaCl (3M), Biologic USA, LLC, Knoxville, TN, USA) as the reference electrode, and a graphite rod as the counter electrode. Two separated reference electrodes were used for electrodeposition and cyclic voltammetry (CV) experiments. A scan rate of 20 mV/s or 100 mV/s was used for CV experiments with a 1 mV/s sampling interval. All CV experiments were performed in a quiescent solution. The investigation of glucose sensing was done using chronoamperometry. All amperometry data (i-t curve) were collected 10 min after the settling period, unless stated otherwise. The amperometry experiment was performed at a specified potential versus Ag/AgCl/3 M NaCl, with a 0.3 s sampling interval. All amperometry was performed in a solution stirred at 240 rpm and in a Faraday cage. Amperometry was also used to test the stability of the fabricated biosensors. The biosensors were stored dry in an oven at 37 °C when

For experiments in biological fluids, a Au-RuNP nanocomposite was used as the working electrode. Ag/AgCl ink and PtNP nanocomposite ink were printed as reference and counter electrode, respectively, as shown in Figure 1a. For each measurement, the three-electrode system was completely covered by 50 μ L of the sample. ³⁵ For each sample, 40 μ L of whole blood or serum was mixed with 10 μ L of DI water with varying glucose concentrations, which produced different final glucose concentrations in the whole blood and human serum.

Surface Characterization. The surface morphology of the nanocomposite and Au-RuNP nanocomposite was observed using field-emission scanning electron microscopy (FESEM, S-4800, Hitachi, Japan). The morphology of the MWCNT and PtNP base was also

characterized by transmission electron microscopy (TEM, Tecnai G2 20, FEI Company, OR). The elemental composition was determined using energy dispersive X-ray spectroscopy (EDX) attached to the FESEM system. The element and chemical composition of the Au-RuNP surface was further characterized by X-ray photoelectron spectroscopy (XPS) using a Kratos AXIS ultra-delay-line detector (DLD) imaging X-ray photoelectron spectrometer.

Synthesis of PtNP-MWCNT-Based Nanocomposite. To create the MWCNT-based nanocomposite, 25.32 mg of carboxylic-functionalized MWCNTs (1 wt %) and 126.58 mg of PtNPs (5 wt %) were first mixed with $582\,\mu\text{L}$ (11 wt %) of DMSO in a sonication bath for 2 h. The mixture was then added to 2000 mg of PEDOT:PSS ink. The mixture was then transferred to a planetary centrifugal mixer (ARE-310, Thinky U.S.A., Inc., Laguna Hills, CA) and mixed for 1 h. Finally, 379.75 mg (16 wt %) of Ecoflex was added, and the mixture was mixed for 10 min and degassed using a planetary centrifugal mixer for 1 h. The final mixture was dried at 60 °C in a vacuum for 1 h to remove the excess DMSO and to reach the desired viscosity for printing.

Direct Ink Writing of the Nanocomposite Electrode. The fabrication process utilized direct ink writing with conductive inks by using a commercial automated fluid dispensing system (Pro-EV 3, Nordson EFD, East Providence, RI). A custom glass capillary pipet with a 30 μ m diameter tip was fabricated to dispense microscale features. The nanocomposite ink was used to define the working electrode, and the conductive traces. The silver Ag ink was used to print the contact pads. PDMS was then printed over the device to insulate the biosensor, leaving only the working electrode exposed for electrochemical activity. By using a direct ink writing technique and our nanocomposite ink, the nonenzymatic glucose biosensor can be printed on any available substrate. Figure 1a shows an example of a nonenzymatic biosensor, which was printed on a liquid crystal polymer (LCP) substrate. The nanocomposite working electrode was then used for one-step electrodeposition of Au-RuNPs for the direct oxidation of glucose. Figure 1b on the left presents the nanocomposite surface before the electrodeposition of Au-RuNPs.

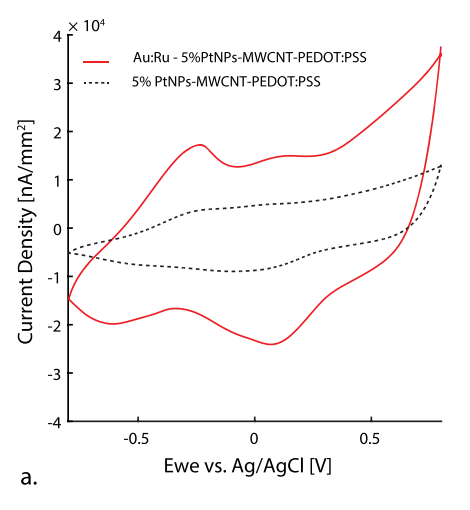
Synthesis of 1:3 Au-Ru Alloy Nanoparticles on a PtNP Nanocomposite Surface. The electrochemical deposition of Au-RuNPs on the nanocomposite was performed in 2.5 mM HAuCl₄ and 7.5 mM RuCl₃ in a 0.2 M H₂SO₄ aqueous solution. Prior to the experiment, a H₂SO₄ solution was deoxygenated with a high purity nitrogen gas for 30 min to remove the oxygen. HAuCl₄ and RuCl₃ were added to the H2SO4 solution, which was then sonicated in an ice bath for complete dissolution (~5 h). The electrodeposition of Au-RuNPs was carried our for 180 s at -0.2 V versus Ag/AgCl. The temperature of the solution was controlled at 4 °C using an ice bath in order to obtain smaller particles. The obtained Au-RuNPs were washed with distilled water and then dried at room temperature. Figure 1b (right) presents the surface of Au-RuNPs after electrodeposition on the nanocomposite electrode. This method was modified from the work by Xiao et al. 36 A different concentration at 3:1 HAuCl₄:RuCl₃ was also tested to optimize for the best condition. As a result, 1:3 HAuCl₄:RuCl₃ was chosen (Figure S1). The electrodeposition time was also optimized between 120, 180, and 300 s (Figure S2). We explored different bimetallic systems such Pt-RuNPs before deciding on Au-RuNPs as the catalyst for nonenzymatic glucose sensor (Figure S3).

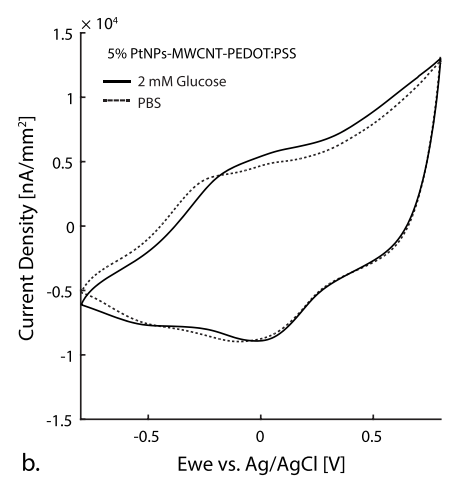
■ RESULTS AND DISCUSSION

Morphological Analysis. We used FESEM and TEM to examine the morphology of the MWCNT-based nanocomposite and the Au-RuNP-modified surface. Figure 2a presents the surface morphology of the resulting nanocomposite before electrodeposition. It displayed a rough morphology, which is likely due to the incorporation of PtNPs into the conductive polymer. We also used TEM to examine the composition of the nanocomposite ink. The inset of Figure 2a presents the morphology of PtNPs in the MWCNT framework. TEM confirmed that PtNPs were aggregates of particles less than 50 nm in diameter. After the electrodeposition of Au-RuNPs on the surface of the nanocomposite, we used FESEM again to reexamine the modified surface. Figure 2b shows the deposition of Au-RuNPs onto the surface. The nanoparticles were welldispersed, with an average size of around 50 nm. One of the key attributes associated with the superior electrocatalytic properties of these materials is high surface area because it increases molecular adsorption, O2 reduction, and pseudocapacitive behavior. 37,38 As such, the nanoporous morphology of our nanocomposite aggregate may improve the sensor perform-

Next, we characterized the elemental composition of the Au-RuNP-modified surface using EDX (Figure 2c), which showed the weight percentage of each material. The EDX spectrum shows large peaks corresponding to Au (35.8 wt %), Ru (0.8 wt %), and Pt (13.7 wt %). The spectrum also has peaks corresponding to C, O, S, and Si, which indicates the presence of PEDOT:PSS and MWCNTs in the sample.

The XPS also confirmed the presence of Au and Ru (Figure 2d-f). The survey scan contains a graphitic C 1s peak at 282.1 eV, which overlaps with Ru 3d peaks. The XPS spectrum of the Au 4f core displays major peaks at 81.5 eV, corresponding to the binding energy of Au 4f_{7/2}, and 85.2 eV, corresponding to the binding energy of Auf_{5/2} (Figure 2d). The XPS analysis is consistent with reports for Au 4f⁴¹ and indicates the successful formation of Au on the surface. XPS spectra for C 1s-Ru 3d core appear in Figure 2e. The C 1s peak corresponds to the sp² carbon atom, which occurs at 282.1 eV. All This peak consists of several overlapping individual peaks belonging to C 1s and Ru 3d_{3/2} photoelectrons. The other distinct peak at 279 eV corresponds to the binding energy of Ru 3d_{5/2} of metallic Ru. These results suggest the successful deposition of AuRu on the surface of the nanocomposite.





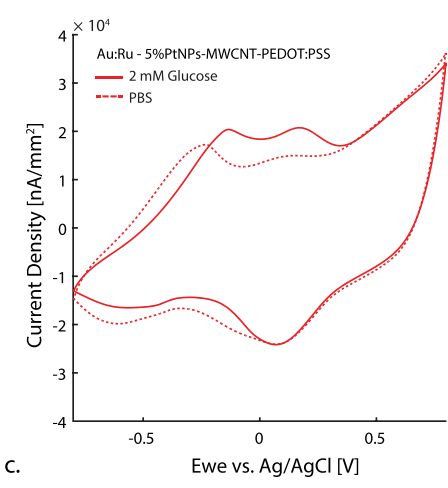


Figure 3. (a) Cyclic voltammetry images of a PtNP-MWCNT-based nanocomposite and Au-RuNP-based nanocomposite biosensors in 0.01 M PBS (pH 7.4). Scan rate = 20 mV/s. (b) Cyclic voltammetry images of the nanocomposite biosensors in 2 mM glucose. Scan rate = 20 mV/s. (c) Cyclic voltammetry images of Au-RuNP-based nanocomposite biosensors. Scan rate = 20 mV/s.

Although the amount of Ru nanoparticles was small at the surface of the biosensors (Figure 2e), their presence was critical in creating the synergistic effects with Au nanoparticles to enable glucose measurements at -0.1 V and prevent electroactive interferences. As shown in Figure S4, the nanocomposite

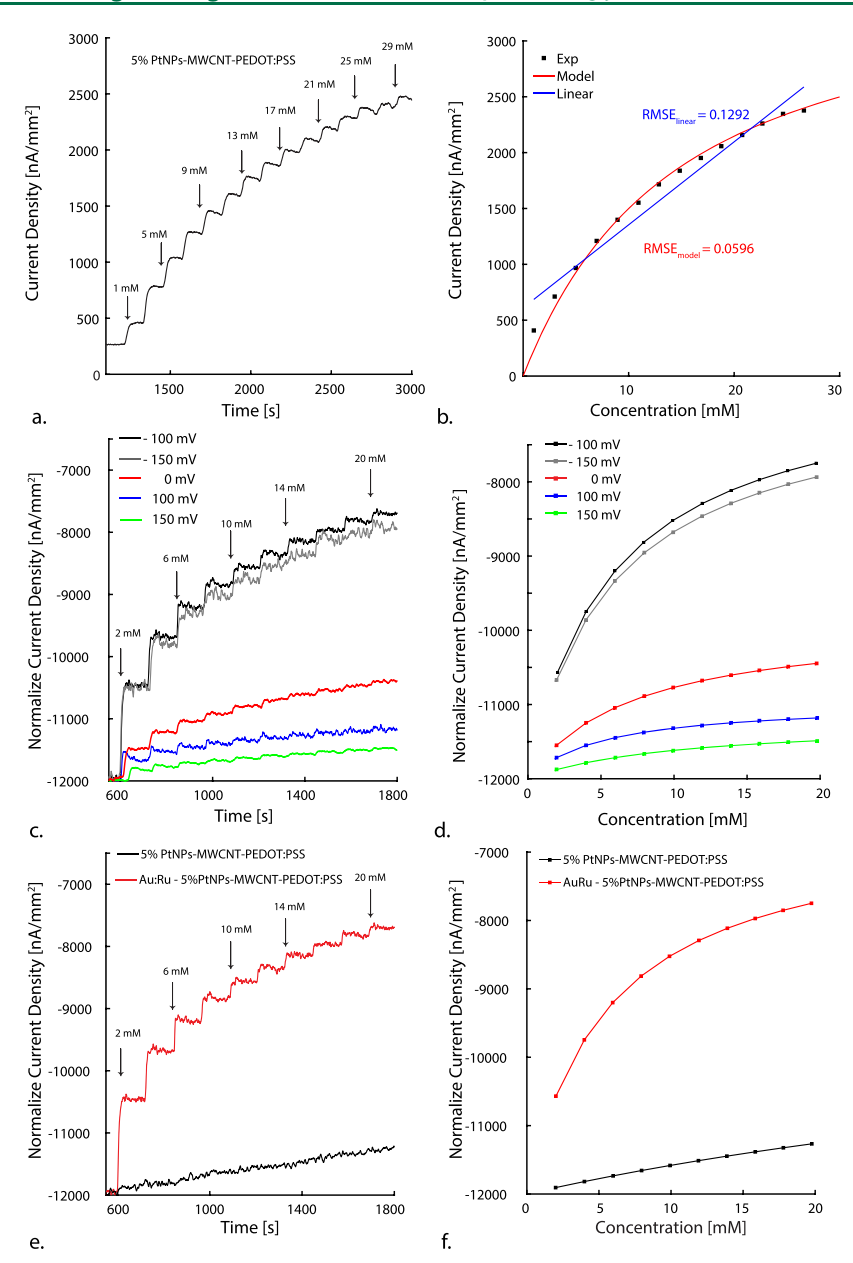


Figure 4. (a) Current—time curve obtained using our nanocomposite biosensor with the successive addition of glucose from 1 mM up to 29 mM with every 2 mM increment in 0.01 M PBS (pH 7.4). (b) Linear fit for glucose using the nanocomposite electrode compared to the nonlinear model of the steady-state response of the nanocomposite glucose sensor. (c) Current—time curve obtained with the Au-RuNP-based nanocomposite biosensor with the successive addition of glucose with every 2 mM increment in 0.01 M PBS (pH 7.4) at different potentials. (d) Nonlinear feature of the steady-state response for glucose with the Au-RuNP-based nanocomposite electrode at different potentials. (e) Current—time curve obtained with the Au-RuNP-based nanocomposite biosensor and the nanocomposite with the successive addition of glucose at 2 mM increments in 0.01 M PBS (pH 7.4) at —0.1 V. (f) Nonlinear feature of the steady-state response for glucose with the Au-RuNP-based nanocomposite biosensor and the nanocomposite with the successive addition of glucose in 0.01 M PBS (pH 7.4) at —0.1 V.

Table 1. List of Key Fitting Parameters in the Simulation for Each Respective Experiment

	type	N_0	$k_{\rm F} \left(m^3/{\rm s/mol}\right)$	$k_{\rm R} \left(1/{\rm s}\right)$	$k'_{\rm R} \left(1/{ m s}\right)$
Figure 4b	nanocomposite only at 0.5 V	2.5×10^{-5}	2.6×10^{-2}	0.064	0.075
Figure 4d	Au-RuNPs at 0.15 V	2.5×10^{-5}	8.5×10^{-2}	0.085	0.819
	Au-RuNPs at 0.1 V	2.5×10^{-5}	8.5×10^{-2}	0.176	0.357
	Au-RuNPs at 0 V	2.5×10^{-5}	8.5×10^{-2}	0.435	0.443
	Au-RuNPs at −0.1 V	2.5×10^{-5}	8.5×10^{-2}	0.435	0.059
	Au-RuNPs at -0.15 V	2.5×10^{-5}	8.5×10^{-2}	0.435	0.044
Figure 4f	Au-RuNPs at -0.1 V	2.5×10^{-5}	8.5×10^{-2}	0.455	0.044
	nanocomposite only at -0.1 V	1.4×10^{-5}	7.7×10^{-3}	0.455	0.044

Table 2. Detection Performances of Non-Enzymatic Glucose Biosensors^a

catalyst	substrate	sensitivity (nA/(µM mm²))	limit of detection (mM)	linear range (mM)	operational potential	selectivity	medium	reference
Pt/Ru/ MWCNTs/IL	GCE/FTO	0.107	0.050	0.2-15	−0.1 vs SCE	AA, UA, AP, fructose	PBS (pH 7.4)	36
PtRu NPs/ MWCNTs	GCE	0.282	0.025	1-15	+0.55 vs Ag/ AgCl	AA, DA, UA	0.1 M NaOH	55
PtAu/MWCNT	thin film Pt and Au	0.107	0.010	24.4	+0.3 vs Ag/ AgCl	AA,UA,AP	PBS (pH 7.4)	56
PtAu/C nanocomposite	GCE	0.047	0.002	0-10	+0.35 vs Ag/ AgCl	AA,UA,AP, DA	PBS (pH 7.4)	57
PtAu/C powder Nafion	GCE	0.128	0.001	0.2-4.8	+0.35 vs Ag/ AgCl	AA, DA, UA	PBS (pH 7.4)	58
PtAu/Nanofiber	BDD/Si wafer	N/A	0.006	0.01-7.5	-0.15 vs Ag/AgCl	AA, AP, UA, NaCl	PBS (pH 7.4)	16
PtRu-PtSn	GCE	N/A	0.700	0.0001-4	-0.1 vs Ag/ AgCl	AA, UA	0.1 M NaOH	59
PtPd	GCE	0.001	0.120	1-2.5	−0.02 vs Ag/AgCl	AA, UA, AP	PBS (pH 7.4)	60
PtAu nanocorals	GCE	0.021	0.028	22	+0.4 vs Ag/ AgCl	AA, UA	PBS (pH 7.4)	61
Au-RuNPs	PtNPs-MWCNT nanocomposite	0.234	0.068	10	-0.1 vs Ag/ AgCl	AA, UA, AP, fructose, sucrose, lactose	PBS (pH 7.4)	this work

[&]quot;Abbreviations: N/A, not applicable; AA, ascorbic acid; UA, uric acid; AP, 4-acetamidophenol; DA, dopamine.

surfaces that were deposited with only Au nanoparticles were not able to detect glucose at -0.1 V. Moreover, we varied the RuCl $_3$ concentration in an electrodeposited solution and assessed the biosensors catalytic performances to further analyze the role of the RuNPs. Figure S5a and b exhibit CVs of the AuNP nanocomposite, Au-RuNP (1:3) nanocomposite, and Au-RuNP (1:5) nanocomposite in a solution of 0.01 M PBS (pH 7.4) and 2 mM glucose at a scan rate of 20 mV/s. The Au-RuNP (1:5) electrode showed the highest currently density compared to the other electrodes in the PBS solution. However, in glucose-spiked samples, the anodic peak at -0.1 V, which is considered to be related to the direct electrooxidation of glucose, was the highest for Au-RuNPs (1:3). Thus, we used this composition as our electrode material to fabricate our nonenzymatic glucose biosensor.

Electrocatalytic Activity for Glucose Oxidation in Neutral Media. We assessed the catalytic performance of Au-RuNPs toward glucose oxidation in neutral media. Figure 3a shows CVs of the nanocomposite and Au-RuNP-modified electrode in a solution of 0.01 M PBS (pH 7.4) at a scan rate of 20 mV/s. The Au-RuNP electrode exhibited higher current density values and a greater catalytic behavior than samples without Au-RuNPs. We also compared the CV profile of the nanocomposite in the presence of glucose at scan rate of 20 mV/s (Figure 3b). The nanocomposite exhibited anodic peaks at approximately -0.4, +0.2, and +0.6 V versus Ag/AgCl, which can be attributed to the multielectron transfer of glucose oxidation on the nanocomposite surface.

After depositing Au-RuNPs, we saw two distinct cathodic reduction peaks at +0.05 V and -0.5 V. Previous studies on the electrocatalytic oxidation of organic molecules on bimetallic systems of noble metals have proposed a "bi-function mechanism", in which Ru dissociates water, leaving adsorbed OH species (Ru(OH)_{ads}).^{47–49} As such, we predicted that Ru(OH)_{ads} reacted with Au to form gold hydroxide in the solution. ⁴⁷ Figure 3c shows that in 2 mM glucose in 0.01 M PBS (pH 7.4), Au-RuNPs show a high electroactivity toward glucose oxidation. We observed a large anodic peak at around +0.2 V from the forward scan, which suggests that the electrooxidation

of glucose with Au-RuNPs may consist of multistep electrode reactions. $^{10,47}\,$

In addition, there is an anodic peak around -0.1 V, which is generally considered to be related to the direct electrooxidation of glucose adsorbed onto the catalyst. Figure 1c and Figure 1d show a possible mechanism of direct glucose oxidation on the surface of Au-RuNPs. Eqs 1-4 describe possible chemical reactions between the metal nanoparticle surface and glucose molecules. Ru(OH)_{ads} species with many active sites on their surfaces would reduce the energy of OH⁻ adsorption onto Au, leading to the enhancement of the direct electrooxidation of glucose corresponding to the anodic peak at around -0.1 V.

$$C_6H_{12}O_6 + RuOH \xrightarrow{k_F} Ru[C_6H_{11}O_6]_{ads} + H_2O$$
 (1)

$$C_6H_{12}O_6 + AuOH \xrightarrow{k_F} Au[C_6H11O_6]_{ads} + H_2O$$
 (2)

$$Ru + OH^{-} \underset{k'_{R}}{\overset{k_{R}}{\rightleftharpoons}} RuOH + e^{-}$$
(3)

$$Au + OH^{-} \underset{k'_{R}}{\overset{k_{R}}{\rightleftharpoons}} AuOH + e^{-}$$
(4)

Nonlinear Analytical Model. A linear approximation does not hold for a two-step reaction of the electrocatalytic oxidation of glucose, which includes oxidative adsorption of intermediates and follows with their oxidation. Furthermore, the geometrical and chemical features of sensors greatly impacts the linearity of the biosensor response. Therefore, it is necessary to have an accurate nonlinear model to explain the sensitivity of nonenzymatic glucose sensors. Recently, an analytical model has been developed, which attributed the linear range to the intrinsic properties of different reaction mechanisms. ⁵⁰

In this study, a modified Butler—Volmer model was used and applied to our specific nanostructure surface. Au-RuNP nonenzymatic glucose detection is modeled as the two-step process described above (eqs 1–4). In this case, $k_{\rm F}$ represents the forward reaction rate, while $k_{\rm R}$ and $k_{\rm R}'$ represent the forward and reverse reaction constants, respectively, in eq 2 and 3. $k_{\rm R}$ and

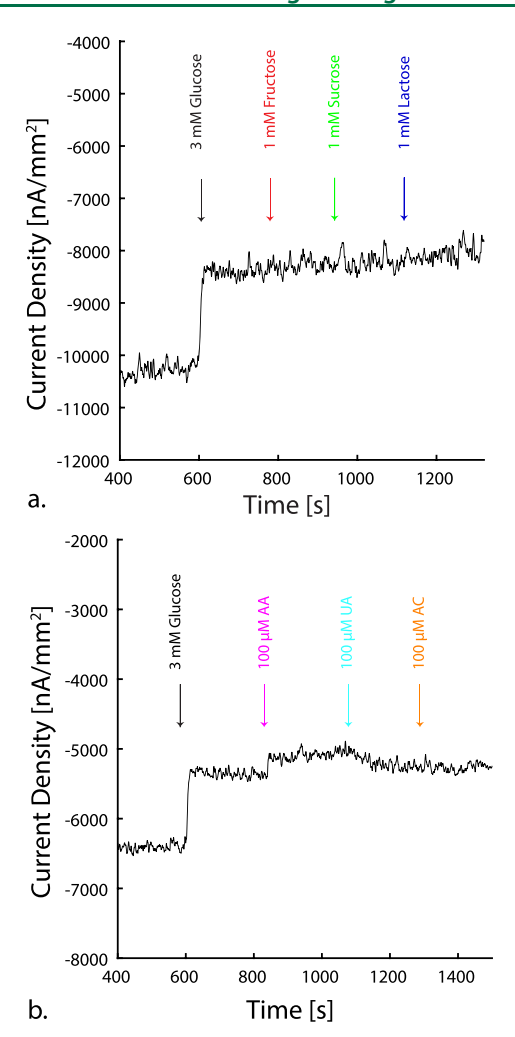


Figure 5. (a) Interference study for the Au-RuNP-based nanocomposite in 0.01 M PBS (pH 7.4) with the successive addition of glucose, fructose, sucrose, and lactose. (b) Interference study for the Au-RuNP-based nanocomposite in 0.01 M PBS (pH 7.4) with the successive addition of glucose, AA, UA, and AP.

 $k_{\rm R}'$ follow the Butler–Volmer equation with an electrode bias potential.

The model applies classical diffusion in eq 5. Eqs 5 and 6 quantify the mass transport of glucose, which is a diffusion-limited process in bulk solution, before they reach the electrode surface. In this case, natural convection from secondary transport phenomena is not considered. Since Au-RuNPs are immobilized on the nanocomposite electrode surface, the oxidation reaction only happens when glucose molecules diffuse near the electrode surface. Reaction flux is described in eq 6, and the surface glucose absorption flux is defined as

$$\frac{\mathrm{d}G}{\mathrm{d}t} = D\nabla^2 G \tag{5}$$

$$J_{\rm rec} = k_{\rm F} N_{\rm M} G_{\rm s} \tag{6}$$

with the glucose diffusion coefficient in the bulk sample solution D, glucose concentration G, surface density of metal nanoparticles $N_{\rm M}$, and the bulk glucose concentration near the nanoparticle surface $G_{\rm s}$. In eq 7, the reaction flux $J_{\rm rec}$ was coupled with the electrode surface density of ${\rm Au}({\rm OH})_{\rm ads} - {\rm Ru}({\rm OH})_{\rm ads}$, which can be presented as the sum of the forward and reverse reaction flux:

$$\frac{\mathrm{d}N_{\mathrm{M-OH}}}{\mathrm{d}t} = k_{\mathrm{F}}N_{\mathrm{M}}G_{\mathrm{s}} - (k_{\mathrm{R}}'N_{\mathrm{M-OH}}) \tag{7}$$

where $N_{\rm M}$ and $N_{\rm M-OH}$ represent the surface densities of Au–Ru (M) and Au(OH)_{ads}–Ru(OH)_{ads} (M–OH), respectively, which follow the total metal elements conservation N_0 :

$$N_{\rm M} + N_{\rm M-OH} = N_0 \tag{8}$$

It is worth mentioning that pH plays an important role in nonenzymatic glucose sensing systems. Many studies have been conducted at pH > 9 to ensure sufficient OH⁻ supply for the chemical reactions. Consequently, the concentration of OH⁻ is not the rate-limiting factor but the surface density of $M(OH)_{ads}$, N_{M-OH} . Therefore, in our model, pH-dependence is not included. Moreover, all of the experiments in this study were conducted in PBS at pH 7.4. The model can be solved analytically to find the coupled diffusion and surface reaction rates from eqs 5–8. By applying "diffusion equivalent capacitance", ⁵¹ the steady-state diffusive flux of glucose in a bulk solution can be written as

$$J_{\text{diff}} = C_{\text{D}} \cdot \frac{G_0 - G_{\text{s}}}{A_{\text{e}}} \tag{9}$$

where $C_{\rm D}$ is the equivalent diffusion capacitance for the nanostructured electrode, $G_{\rm s}$ is the glucose concentration near the electrode surface, G_0 is the bulk glucose concentration, 50,52 and $A_{\rm e}$ represents the surface area of a single nanoelectrode. The sensor response can be obtained by solving eqs 5–9 and rewriting the equations in a normalized form with unitless variables: $N_{\rm M}^* = \frac{N_{\rm M}}{N_0}$, $N_{\rm M-OH}^* = \frac{N_{\rm M-OH}}{N_0}$, $G_{\rm s}^* = \frac{G_{\rm s}}{G_0}$, $\gamma = \frac{C_{\rm D}}{A_{\rm e}k_{\rm F}N_0}$, $\alpha = \frac{k_{\rm R}}{k_{\rm F}G_0'}$, and $\beta = \frac{k_{\rm K}'}{k_{\rm F}G_0}$. More information on the exact solution can be found in a recent study from Jin et al., 2019.

Unknown variables N_{M}^* , $N_{\text{M-OH}}^*$, and G_s^* can be solved with an approximated expression for N_{M}^* and $N_{\text{M-OH}}^*$:

$$N_{\rm M}^* \approx \frac{\alpha}{(\alpha + \beta + 1) - \frac{\alpha}{\gamma}}$$
 (10)

$$N_{\rm M-OH}^* = 1 - N_{\rm M}^* \approx \frac{G_0 + \left(\frac{k_{\rm K}'}{k_{\rm F}} - \frac{A_{\rm e}k_{\rm R}N_0}{C_{\rm D}}\right)}{G_0 + \left(\frac{k_{\rm R} + k_{\rm K}'}{k_{\rm F}} - \frac{A_{\rm e}k_{\rm R}N_0}{C_{\rm D}}\right)}$$
(11)

The final amperometric response of the glucose sensor can be expressed as a function of $N_{\rm M-OH}$:

$$j = i/A_{\text{eff}} = q \cdot N_{\text{A}} \cdot (k_{\text{R}} N_{\text{M-OH}} - k_{\text{R}}' N_{\text{M}}) \approx q \cdot N_{\text{A}} \cdot (k_{\text{R}} + k_{\text{R}}') \cdot N_{0} \cdot \left(N_{\text{M-OH}}^{*} - \frac{k_{\text{R}}'}{k_{\text{R}} + k_{\text{R}}'}\right)$$
(12)

 $A_{\rm eff}$ describes the effective electrode surface area, and $N_{\rm A}$ is the Avogadro constant. On the basis of this model, the steady-state amperometric response of the Au-RuNP nonenzymatic sensors was modeled and is presented as solid lines in Figure 4b, Figure 4d, and Figure 4f.

Amperometric Response of Fabricated Biosensors for Nonenzymatic Glucose Detection. We first investigated amperometric glucose sensing using the nanocomposite electrode (Figure 4a and Figure 4b). The nanocomposite at +0.5 V was able to nonenzymatically sense glucose in 0.01 M PBS (pH 7.4). Figure 4b takes this calibration data and compares a linear fit to the nonlinear model. The root-mean-

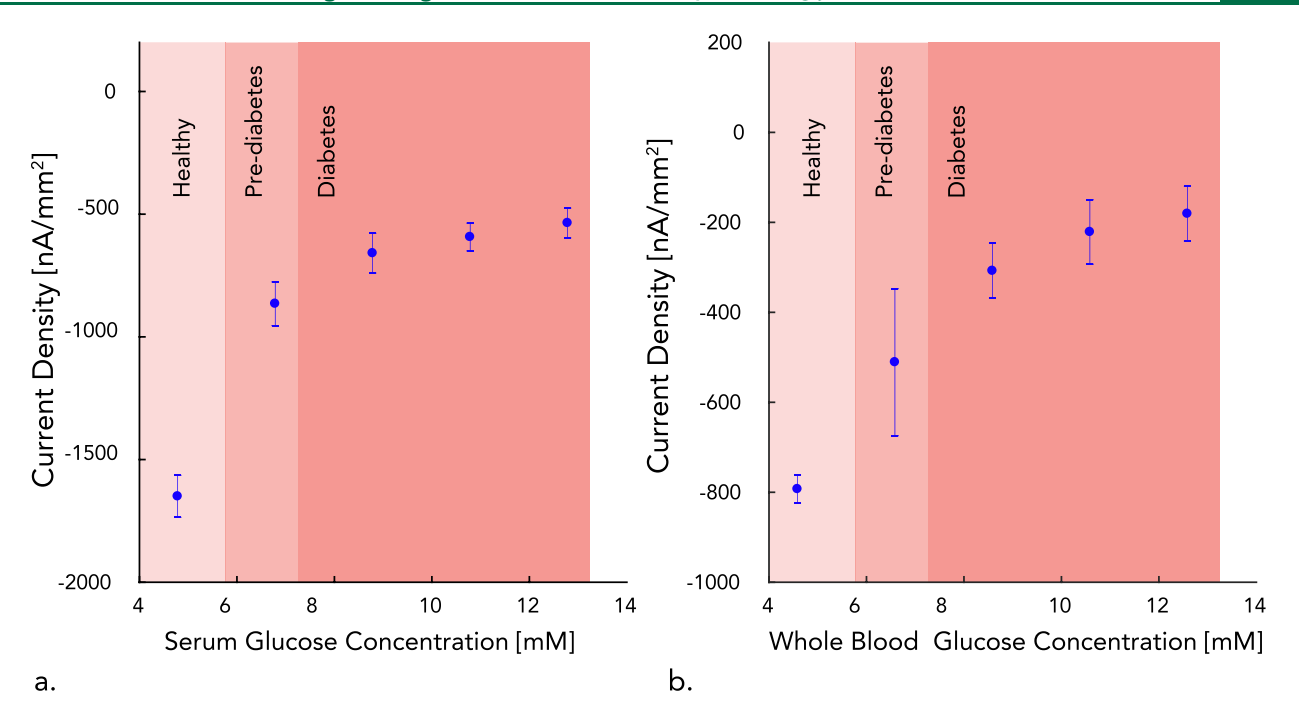


Figure 6. Nonlinear feature of the steady-state response for glucose with the Au-RuNP-based nanocomposite biosensor to different glucose concentrations in (a) human serum and (b) porcine whole blood (n = 4) with a detection potential of -0.1 V versus Ag/AgCl. The stabilization time of the chronoamperometry is 4 min.

square error (RMSE) of the physics-based model is 0.0596, much less than the RMSE of a conventional linear fit of 0.1292. However, at this operating potential, the nanocomposite oxidizes interferents such as AA and AP much faster than it oxidizes glucose. We predicted that the Au-RuNP-modified electrode would have better selectivity than the nanocomposite alone.

In order to find an optimum operating potential, we calibrated the Au-RuNP biosensor at various potentials from -0.15 to +0.15 V to glucose in 0.01 M PBS (pH 7.4) (Figure 4c). We found that the bias potential of -0.1 V versus Ag/AgCl resulted in the greatest sensitivity. Figure 4d shows the impact of the electrode voltage bias by fitting the data from Figure 4c to the nonlinear model. In this case, the surface density of Au–Ru, N_0 , and the forward reaction constant remain the same, while the voltage-dependent reaction constants, k_R and k_R' , change as shown in Table 1. At the optimum electrode bias potential, -0.1 V, k_R is maximized, and k_R' is minimized. Therefore, we chose -0.1 V as the optimal potential for amperometric glucose sensing with Au-RuNP biosensors.

Figure 4e shows the current response of Au-RuNPs and the nanocomposite to glucose while calibrated at -0.1 V versus Ag/AgCl. Figure 4f shows the steady-state amperometric response for both catalysts at a -0.1 V potential and the effect of adding Au-RuNPs on the surface of the nanocomposite. Au-RuNPs had a higher sensitivity compared to the nanocomposite alone. Table 1 shows that adding Au-RuNPs increases both the total metal catalyst density, N_0 , and the forward reaction constant, $k_{\rm F}$.

Eq 12 may be used for calibrations over the full range of glucose concentrations, allowing the estimation of the uncertainty or saturation limit of the output current. On the other hand, a reasonable linear relationship between the steady state current and glucose concentration can be established between 1 and 10 mM with a sensitivity of 0.2347 nA/(μ M mm²) \pm 0.0198 (n = 3). The limit of detection was calculated to

be 0.068 mM (signal-to-noise, S/N = 3). Table 2 compares our nonenzymatic glucose biosensor to previously reported nonenzymatic glucose biosensors.

Selectivity, Reproducibility, Stability, Reusability, and Performance in Biological Fluids. The selectivity of nonenzymatic-based glucose sensors is a challenge due to the lack of a specific biorecognition agent. Figure 5a shows that the Au-RuNP biosensor was selective to glucose over other sugars, including fructose, sucrose, and lactose. We also evaluated the response of our biosensor physiological levels of ascorbic acid (AA), uric acid (UA), and 4-acemitadophenol (AP). As seen in Figure 5b, there is negligible interference from AA, UA, or AP. The selectivity of the nonenzymatic glucose sensor is a result of the lower operating potential used, below the peak oxidation potentials of the interferents.

Next, we evaluated the reproducibility and stability of our nonenzymatic glucose sensors. We tested the amperometric responses of 5 different Au-RuNP biosensors to 2 mM glucose independently and measured a relative standard deviation (RSD) value of 3.87%. We investigated the long-term stability of the sensors by monitoring the changes in biosensor sensitivity over 3 weeks. We stored the biosensors in an oven at 37 °C when not in-use. Our results showed that biosensors maintained more than 87% of their sensitivity to 2 mM glucose after 3 weeks (Figure S6). This suggests that our nonenzymatic glucose sensor has a long-term stability at body temperature. Thus, we concluded our Au-RuNP-modified electrode is suitable for the fabrication of sensitive, repeatable, and stable nonenzymatic amperometric glucose sensors.

We also evaluated the reusability of the biosensor by calibrating the device multiple times at various glucose concentrations. In general, we observed decreased current responses with each calibration. However, we were also able to electrochemically regenerate the biosensor using five cycles of CVs (0 and 1.5 V in 0.5 M H₂SO₄ with a scan rate of 100 mV/

s). 35,53 Figure S7 shows a comparison of the normalized current density between the first and seventh calibration of our biosensor (n = 5). We believe this result demonstrates the stability of our low-cost biosensor (Figure S4) and their potential application in a closed system that allows surface regeneration (i.e., lab-on-a-chip). 35,54

Finally, we measured the glucose concentration from human serum and porcine whole blood samples directly using our biosensors at various simulated prediabetic and diabetic conditions. Figure 6 shows the amperometric responses for various glucose concentrations at a -0.1 V potential in human serum and porcine whole blood (n = 4 each). We saw substantial changes in current responses between health an prediabetic ranges in both serum and blood. We believe these results demonstrate the capability of our biosensors to differentiate physiologically relevant glucose concentrations in biological media. By taking the nonlinear responses of these nonenzymatic biosensors into account, we may also be able to improve the range and performance of these biosensors for future in vitro and in vivo diagnostic applications.

CONCLUSION

In summary, we have successfully developed a nonenzymatic glucose sensor using a one-step electrodeposition of Au-RuNPs on MWCNT-based nanocomposites. The nanocomposite electrodes were fabricated using a rapid and template-free method. In this study, direct glucose oxidation on the nanocomposite electrode was investigated both using voltammetric and amperometric methods. Additionally, a nonlinear model was used to correlate the geometrical and chemical design parameters to the nonlinear response of the glucose sensor. The Au-RuNP electrode gave a good current response to glucose, owing to its high active surface area and the synergistic effect of Au and Ru on the surface, as well as due to PtNPs and MWCNTs underneath. The fabricated sensor also provided good reproducibility, selectivity, and stability for glucose determination, which are necessary attributes for future in vivo and other applications.

ASSOCIATED CONTENT

Supporting Information

The Supporting Information is available free of charge at https://pubs.acs.org/doi/10.1021/acsbiomaterials.0c00647.

Current-time curve and nonlinear feature of the steadystate response for glucose with Au-RuNP biosensors with two different electrodeposition concentrations of HAuCl₄ to RuCl₃; summary of key fitting parameters in the simulation for the experiment with two different electrodepositing concentrations of HAuCl₄ to RuCl₃; currenttime curve and nonlinear feature of the steady-state response for glucose with Au-RuNP biosensors with different electrodepositing times; summary of key fitting parameters in the simulation for the experiment with different electrodepositing times; current-time curve and nonlinear feature of the steady-state response for glucose with Au-RuNP biosensors with two different bimetallic systems; summary of key fitting parameters in the simulation for the experiment with two different bimetallic systems; current-time curve and nonlinear feature of the steady-state response for glucose with Au-RuNP biosensors and Au nanocomposite biosensors; cyclic voltammetry of the Au-RuNP-based (1:3) nanocomposite, Au-RuNP-based (1:5) nanocomposite, and Au-based nanocomposite biosensors; biosensor lifetime measurement; nonlinear feature of the steady-state response for glucose with Au-RuNP-based nanocomposite biosensors through continuous calibration cycles (PDF)

AUTHOR INFORMATION

Corresponding Author

Hyowon Lee — Weldon School of Biomedical Engineering, Birck Nanotechnology Center, Center for Implantable Devices, Purdue University, West Lafayette, Indiana 47907, United States; orcid.org/0000-0001-7628-1441; Email: hwlee@purdue.edu

Authors

Tran N. H. Nguyen — Weldon School of Biomedical Engineering, Birck Nanotechnology Center, Center for Implantable Devices, Purdue University, West Lafayette, Indiana 47907, United States; orcid.org/0000-0002-6361-9324

Xin Jin — School of Electrical and Computer Engineering, Purdue University, West Lafayette, Indiana 47907, United States;
ocid.org/0000-0002-4117-4344

James K. Nolan — Weldon School of Biomedical Engineering, Birck Nanotechnology Center, Center for Implantable Devices, Purdue University, West Lafayette, Indiana 47907, United States

Jian Xu — Weldon School of Biomedical Engineering, Birck Nanotechnology Center, Center for Implantable Devices, Purdue University, West Lafayette, Indiana 47907, United States

Khanh Vy H. Le — Weldon School of Biomedical Engineering, Birck Nanotechnology Center, Center for Implantable Devices, Purdue University, West Lafayette, Indiana 47907, United States

Stephanie Lam — Weldon School of Biomedical Engineering, Birck Nanotechnology Center, Center for Implantable Devices, Purdue University, West Lafayette, Indiana 47907, United States

Yi Wang — Weldon School of Biomedical Engineering, Birck Nanotechnology Center, Center for Implantable Devices, Purdue University, West Lafayette, Indiana 47907, United States

Muhammad A. Alam — School of Electrical and Computer Engineering, Purdue University, West Lafayette, Indiana 47907, United States

Complete contact information is available at: https://pubs.acs.org/10.1021/acsbiomaterials.0c00647

Note

The authors declare no competing financial interest.

ACKNOWLEDGMENTS

This work was supported in part by the National Science Foundation (United States), under grants ECCS-1944480 and CNS-1726865, and by the Global Research Outreach program of the Samsung Advanced Institute of Technology. We would like to thank Dr. Dmitry Zemlyanov for conducting XPS at the Surface Analysis Facility of the Birck Nanotechnology Center, Purdue University.

REFERENCES

- (1) Zhu, C.; Yang, G.; Li, H.; Du, D.; Lin, Y. Electrochemical Sensors and Biosensors Based on Nanomaterials and Nanostructures. *Anal. Chem.* **2015**, *87*, 230–249.
- (2) American Diabetes Association. Diagnosis and Classification of Diabetes Mellitus. *Diabetes Care* **2010**, 33, S62–S69.

- (3) Nichols, S. P.; Koh, A.; Storm, W. L.; Shin, J. H.; Schoenfisch, M. H. Biocompatible Materials for Continuous Glucose Monitoring Devices. *Chem. Rev.* **2013**, *113*, 2528–2549.
- (4) Shaw, J. E.; Sicree, R. A.; Zimmet, P. Z. Global Estimates of The Prevalence of Diabetes for 2010 and 2030. *Diabetes Res. Clin. Pract.* **2010**, 87, 4–14.
- (5) Wilson, R.; Turner, A. P. F. Glucose Oxidase: an Ideal Enzyme. *Biosens. Bioelectron.* **1992**, *7*, 165–185.
- (6) Park, S.; Boo, H.; Chung, T. D. Electrochemical Non-enzymatic Glucose Sensors. *Anal. Chim. Acta* **2006**, *556*, 46–57.
- (7) Si, P.; Huang, Y.; Wang, T.; Ma, J. Nanomaterials for Electrochemical Non-enzymatic Glucose Biosensors. *RSC Adv.* **2013**, 3.3487–3502.
- (8) Hwang, D. W.; Lee, S.; Seo, M.; Chung, T. D. Recent Advances in Electrochemical Non-enzymatic Glucose Sensors-A Review. *Anal. Chim. Acta* **2018**, *1033*, 1–34.
- (9) Bae, J. H.; Han, J. H.; Chung, T. D. Electrochemistry at Nanoporous Interfaces: New Opportunity for Electrocatalysis. *Phys. Chem. Chem. Phys.* **2012**, *14*, 448–463.
- (10) Si, P.; Huang, Y.; Wang, T.; Ma, J. Nanomaterials for Electrochemical Non-enzymatic Glucose Biosensors. RSC Adv. 2013, 3, 3487.
- (11) Toghill, K. E.; Compton, R. G. Electrochemical Non-enzymatic Glucose Sensors: A perspective and an evaluation. *Int. J. Electrochem. Sci.* **2010**, *5*, 1246–1301.
- (12) Gollas, B.; Elliott, J. M.; Bartlett, P. N. Electrodeposition and Properties of Nanostructured Platinum Films Studied by Quartz Crystal Impedance measurements at 10 MHz. *Electrochim. Acta* **2000**, *45*, 3711–3724.
- (13) Zhao, S.; Zhang, K.; Bai, Y.; Yang, W.; Sun, C. Glucose Oxidase/Colloidal Gold Nanoparticles Immobilized in Nafion Film on Glassy Carbon Electrode: Direct Electron Transfer and Electrocatalysis. *Bioelectrochemistry* **2006**, *69*, 158–163.
- (14) Yang, J.; Jiang, L. C.; Zhang, W. D.; Gunasekaran, S. A Highly Sensitive Non-enzymatic Glucose Sensor based on a Simple Two-step Electrodeposition of Cupric Oxide (CuO) Nanoparticles onto Multiwalled Carbon Nanotube Arrays. *Talanta* **2010**, *82*, 25–33.
- (15) Wang, J.; Thomas, D. F.; Chen, A. Nonenzymatic Electrochemical Glucose Sensor based on Nanoporous PtPb Networks. *Anal. Chem.* **2008**, *80*, 997–1004.
- (16) Nantaphol, S.; Watanabe, T.; Nomura, N.; Siangproh, W.; Chailapakul, O.; Einaga, Y. Bimetallic Pt-Au Nanocatalysts Electrochemically Deposited on Boron-doped Diamond Electrodes for Nonenzymatic Glucose Detection. *Biosens. Bioelectron.* **2017**, *98*, 76–82.
- (17) Holt-Hindle, P.; Nigro, S.; Asmussen, M.; Chen, A. Amperometric Glucose Sensor based on Platinum-Iridium Nanomaterials. *Electrochem. Commun.* **2008**, *10*, 1438–1441.
- (18) Duan, S.; Wang, R. Bimetallic Nanostructures with Magnetic and Noble Metals and their Physicochemical Applications. *Prog. Nat. Sci.* **2013**, 23, 113–126.
- (19) Yang, J.; Chen, X.; Yang, X.; Ying, J. Y. Stabilization and Compressive Strain Effect of AuCu Core on Pt Shell for Oxygen Reduction Reaction. *Energy Environ. Sci.* **2012**, *5*, 8976–8981.
- (20) Ferrando, R.; Jellinek, J.; Johnston, R. L. Nanoalloys: From Theory to Applications of Alloy Clusters and Nanoparticles. *Chem. Rev.* **2008**, *108*, 845–910.
- (21) Guisbiers, G.; Mejia-Rosales, S.; Khanal, S.; Ruiz-Zepeda, F.; Whetten, R. L.; José-Yacaman, M. Gold-copper Nano-alloy, "Tumbaga", in the Era of Nano: Phase Diagram and Segregation. *Nano Lett.* **2014**, *14*, *6718*–*6726*.
- (22) Hwang, C. B.; Fu, Y. S.; Lu, Y. L.; Jang, S. W.; Chou, P. T.; Wang, C. R.; Yu, S. J. Synthesis, Characterization, and Highly Efficient Catalytic Reactivity of Suspended Palladium Nanoparticles. *J. Catal.* **2000**, *195*, 336–341.
- (23) Wang, X.; Zhu, Y.; Vasileff, A.; Jiao, Y.; Chen, S.; Song, L.; Zheng, B.; Zheng, Y.; Qiao, S. Z. Strain Effect in Bimetallic Electrocatalysts on the Hydrogen Evolution Reaction. *ACS Energy Letters* **2018**, *3*, 1198–1204.

- (24) Mueller, J. E.; Krtil, P.; Kibler, L. A.; Jacob, T. Bimetallic Alloys in Action: Dynamic Atomistic Motifs for Electrochemistry and Catalysis. *Phys. Chem. Chem. Phys.* **2014**, *16*, 15029–15042.
- (25) Hsu, N. Y.; Chien, C. C.; Jeng, K. T. Characterization and Enhancement of Carbon Nanotube-Supported PtRu Electrocatalyst for Direct Methanol Fuel Cell Applications. *Appl. Catal., B* **2008**, *84*, 196–203.
- (26) Sun, Z.; Li, Z.; Huang, C.; Zhao, Y.; Zhang, H.; Tao, R.; Liu, Z. Ultrasonication-assisted Uniform Decoration of Carbon Nanotubes by Various Particles with Controlled Size and Loading. *Carbon* **2011**, *49*, 4376–4384
- (27) Steigerwalt, E. S.; Deluga, G. A.; Lukehart, C. M. Pt-Ru/carbon fiber nanocomposites: Synthesis, characterization, and performance as anode catalysts of direct methanol fuel cells. A search for exceptional performance. *J. Phys. Chem. B* **2002**, *106*, 760–766.
- (28) Gallego, J.; Tapia, J.; Vargas, M.; Santamaria, A.; Orozco, J.; Lopez, D. Synthesis of Graphene-coated Carbon Nanotubes-Supported Metal Nanoparticles as Multifunctional Hybrid Materials. *Carbon* **2017**, *111*, 393–401.
- (29) Nguyen, T. N.; Nolan, J.; Cheng, X.; Park, H.; Wang, Y.; Lam, S.; Lee, H.; Kim, S. J.; Shi, R.; Chubykin, A. A.; Lee, H. Fabrication and Ex Vivo Evaluation of Activated Carbon-Pt Microparticle Based Glutamate Biosensor. *J. Electroanal. Chem.* **2020**, *866*, 114136.
- (30) Nolan, J. K.; Nguyen, T. N.; Le, K. V. H.; DeLong, L. E.; Lee, H. Simple Fabrication of Flexible Biosensor Arrays Using Direct Writing for Multianalyte Measurement from Human Astrocytes. *SLAS Technology* **2020**, *25*, 33–46.
- (31) Kingston, C.; Zepp, R.; Andrady, A.; Boverhof, D.; Fehir, R.; Hawkins, D.; Roberts, J.; Sayre, P.; Shelton, B.; Sultan, Y.; Vejins, V.; Wohlleben, W. Release Characteristics of Selected Carbon Nanotube Polymer Composites. *Carbon* **2014**, *68*, 33–57.
- (32) Tian, K.; Prestgard, M.; Tiwari, A. A Review of Recent Advances in Nonenzymatic Glucose Sensors. *Mater. Sci. Eng., C* **2014**, *41*, 100–118
- (33) Kim, J. H.; Nam, K. W.; Ma, S. B.; Kim, K. B. Fabrication and Electrochemical Properties of Carbon Nanotube Film Electrodes. *Carbon* **2006**, *44*, 1963–1968.
- (34) Nguyen, T. N.; Nolan, J. K.; Park, H.; Lam, S.; Fattah, M.; Page, J. C.; Joe, H. E.; Jun, M. B.; Lee, H.; Kim, S. J.; Shi, R.; Lee, H. Facile Fabrication of Flexible Glutamate Biosensor using Direct Writing of Platinum Nanoparticle-based Nanocomposite Ink. *Biosens. Bioelectron.* **2019**, *131*, 257–266.
- (35) Márquez, A.; Jiménez-Jorquera, C.; Domínguez, C.; Muñoz-Berbel, X. Electrodepositable alginate membranes for enzymatic sensors: An amperometric glucose biosensor for whole blood analysis. *Biosens. Bioelectron.* **2017**, *97*, 136–142.
- (36) Xiao, F.; Zhao, F.; Mei, D.; Mo, Z.; Zeng, B. Nonenzymatic Glucose Sensor based on Ultrasonic-electrodeposition of Bimetallic PtM (M = Ru, Pd and Au) Nanoparticles on Carbon Nanotubes-ionic Liquid Composite Film. *Biosens. Bioelectron.* **2009**, *24*, 3481–3486.
- (37) Sokolov, S. V.; Tschulik, K.; Batchelor-McAuley, C.; Jurkschat, K.; Compton, R. G. Reversible or Not? Distinguishing Agglomeration and Aggregation at the Nanoscale. *Anal. Chem.* **2015**, *87*, 10033–10039.
- (38) Lang, X.; Hirata, A.; Fujita, T.; Chen, M. Three-dimensional Hierarchical Nanoporosity for Ultrahigh Power and Excellent Cyclability of Electrochemical Pseudocapacitors. *Adv. Energy Mater.* **2014**, *4*, 1301809.
- (39) Lim, C. S.; Tan, S. M.; Sofer, Z.; Pumera, M. Impact Electrochemistry of Layered Transition Metal Dichalcogenides. *ACS Nano* **2015**, *9*, 8474–8483.
- (40) Jiao, X.; Sokolov, S. V.; Tanner, E. E. L.; Young, N. P.; Compton, R. G. Exploring Nanoparticle Porosity using Nano-impacts: Platinum Nanoparticle Aggregates. *Phys. Chem. Chem. Phys.* **2017**, *19*, 64–68.
- (41) Govindasamy, M.; Manavalan, S.; Chen, S.-M.; Rajaji, U.; Chen, T.-W.; Al-Hemaid, F. M. A.; Ali, M. A.; Elshikh, M. S. Determination of Neurotransmitter in Biological and Drug Samples using Gold Nanorods Decorated f-MWCNTs Modified Electrode. *J. Electrochem. Soc.* 2018, 165, B370–B377.

- (42) Xue, J.; Ma, S.; Zhou, Y.; Zhang, Z.; He, M. Facile Photochemical Synthesis of Au/Pt/g-C₃N₄ with Plasmon-enhanced Photocatalytic Activity for Antibiotic Degradation. ACS Appl. Mater. Interfaces **2015**, 7, 9630–9637.
- (43) Agnès, C.; Arnault, J. C.; Omnès, F.; Jousselme, B.; Billon, M.; Bidan, G.; Mailley, P. XPS Study of Ruthenium Tris-bipyridine Electrografted from Diazonium Salt Derivative on Microcrystalline Boron Doped Diamond. *Phys. Chem. Chem. Phys.* **2009**, *11*, 11647–11654.
- (44) Peng, Y.; Pan, W.; Wang, N.; Lu, J. E.; Chen, S. Ruthenium Ion-Complexed Graphitic Carbon Nitride Nanosheets Supported on Reduced Graphene Oxide as High-Performance Catalysts for Electrochemical Hydrogen Evolution. *ChemSusChem* **2018**, *11*, 130–136.
- (45) Wei, G.; Xu, F.; Li, Z.; Jandt, K. D. Protein-promoted Synthesis of Pt Nanoparticles on Carbon Nanotubes for Electrocatalytic Nanohybrids with Enhanced Glucose Sensing. *J. Phys. Chem. C* **2011**, *115*, 11453–11460.
- (46) Rathod, D.; Dickinson, C.; Egan, D.; Dempsey, E. Platinum Nanoparticle Decoration of Carbon Materials with Applications in Non-enzymatic Glucose Sensing. *Sens. Actuators, B* **2010**, *143*, 547–554.
- (47) Yi, Q.; Yu, W.; Niu, F. Novel Nanoporous Binary Au-Ru Electrocatalysts for Glucose Oxidation. *Electroanalysis* **2010**, *22*, 556–563
- (48) Liu, H.; Song, C.; Zhang, L.; Zhang, J.; Wang, H.; Wilkinson, D. P. A Review of Anode Catalysis in The Direct Methanol Fuel Cell. *J. Power Sources* **2006**, *155*, 95–110.
- (49) Seland, F.; Tunold, R.; Harrington, D. A. Impedance Study of Formic Acid Oxidation on Platinum Electrodes. *Electrochim. Acta* **2008**, 53, 6851–6864.
- (50) Jin, X.; Alam, M. Generalized Modeling Framework of Metal Oxide-based Non-enzymatic Glucose Sensor: Concepts, Methods, and Challenges. *IEEE Trans. Biomed. Eng.* **2020**, *67*, *679*–*687*.
- (51) Nair, P. R.; Alam, M. A. Performance Limits of Nanobiosensors. *Appl. Phys. Lett.* **2006**, *88*, 233120.
- (52) Nair, P. R.; Alam, M. A. A Compact Analytical Formalism for Current Transients in Electrochemical Systems. *Analyst* **2013**, *138*, 525–538.
- (53) Lee, W. C.; Kim, K. B.; Gurudatt, N. G.; Hussain, K. K.; Choi, C. S.; Park, D. S.; Shim, Y. B. Comparison of enzymatic and non-enzymatic glucose sensors based on hierarchical Au-Ni alloy with conductive polymer. *Biosens. Bioelectron.* **2019**, *130*, 48–54.
- (54) Economou, A.; Kokkinos, C.; Prodromidis, M. Flexible plastic, paper and textile lab-on-a chip platforms for electrochemical biosensing. *Lab Chip* **2018**, *18*, 1812–1830.
- (55) Li, L. H.; Zhang, W. D.; Ye, J. S. Electrocatalytic Oxidation of Glucose at Carbon Nanotubes Supported PtRu Nanoparticles and its Detection. *Electroanalysis* **2008**, *20*, 2212–2216.
- (56) Ryu, J.; Kim, K.; Kim, H. S.; Hahn, H. T.; Lashmore, D. Intense Pulsed Light Induced Platinum-gold Alloy Formation on Carbon Nanotubes for Non-enzymatic Glucose Detection. *Biosens. Bioelectron.* **2010**, 26, 602–607.
- (57) Singh, B.; Laffir, F.; McCormac, T.; Dempsey, E. PtAu/C based Bmetallic Nanocomposites for Non-enzymatic Electrochemical Glucose Detection. *Sens. Actuators, B* **2010**, *150*, 80–92.
- (58) Wang, J.; Zhao, D.; Xu, C. Nonenzymatic Electrochemical Sensor for Glucose Based on Nanoporous Platinum-Gold Alloy. *J. Nanosci. Nanotechnol.* **2016**, *16*, 7145–7150.
- (59) Kwon, S. Y.; Kwen, H. D.; Choi, S. H. Fabrication of Nonenzymatic Glucose Sensors based on Multiwalled Carbon Nanotubes with Bimetallic Pt-M(M = Ru and Sn) Catalysts by Radiolytic Deposition. *J. Sens.* **2012**, 2012, 784167.
- (60) Bo, X.; Bai, J.; Yang, L.; Guo, L. The Nanocomposite of PtPd Nanoparticles/Onion-like Mesoporous Carbon Vesicle for Nonenzymatic Amperometric Sensing of Glucose. *Sens. Actuators, B* **2011**, 157, 662–668.
- (61) Liu, Y.; Ding, Y.; Zhang, Y.; Lei, Y. Pt-Au Nanocorals, Pt Nanofibers and Au Microparticles Prepared by Electrospinning and

Calcination for Nonenzymatic Glucose Sensing in Neutral and Alkaline Environment. *Sens. Actuators, B* **2012**, *171–172*, 954–961.